Divalent Ion and Thermally Induced DNA Conformational Polymorphism on Single-walled Carbon Nanotubes

Hong Jin,[†] Esther S. Jeng,[†] Daniel A. Heller,[‡] Prakrit V. Jena,[§] Robert Kirmse,[||] Jörg Langowski,[||] and Michael S. Strano*,[†]

Department of Chemical Engineering, Massachusetts Institute of Technology, Building 66, 25 Ames Street, Cambridge, Massachusetts 02139, Department of Physics, University of Illinois-Urbana/Champaign, 600 S. Mathews Avenue, Urbana, Illinois 61801, and Division of Biophysics of Macromolecules, German Cancer Research Center, Im Neuenheimer Feld 580, D-69120, Heidelberg, Germany

Received March 13, 2007; Revised Manuscript Received June 15, 2007

ABSTRACT: Various sequences of single and double stranded DNA can wrap and colloidally stabilize single-walled carbon nanotubes in solution. The binding of divalent ions to these complexes results in a 10 meV emission energy red-shift of the photoluminescence of the nanotube. In this work, this optical modulation is linked to specific secondary structure changes in the adsorbed DNA. Dynamic light scattering is used to rule out aggregation and inter-particle effects. It is observed that the transition can also be induced thermally over the temperature range between 0 and 50 °C without ion addition. Interestingly, we find evidence of the dissociation of a DNA duplex at the surface, as confirmed using both selective dialysis and DNA electrophoresis on a 20% PAGE gel. Consistent with several observations is a mechanism that proceeds via a competitive, stepwise process of partial desorption of the DNA along the length of SWNT. A two-state mathematical model quantitatively describes the equilibrium for various divalent ions binding to DNA adsorbed at the nanotube surface.

Introduction

Semiconducting single-walled carbon nanotubes (SWNT) are rolled graphene rods with diameters around 1 nm and are one of only a few types of molecules that exhibit band gap photoluminescence (PL) in the near-infrared (nIR)[1−4] when dispersed in solution. The fluorescence is completely photostable even at high fluence, unlike conventional fluorophores and even quantum dot systems. Several promising applications of SWNT nIR emission are under investigation, including imaging and electroluminescent devices.[5] We have pioneered their use as optical sensors, both as biomedical devices[6−8] and as subcellular molecular beacons.[1,9]

Toward the latter application, sensors designed to exploit nanotube PL have used either redox chemistry to populate/depopulate the first interband transition, or E_{11} band,[6−8] or have modulated fluorescence wavelength by modifying solution and adsorbate properties.[3,9] The latter has been described as solvatochromism.[10] Generally, when the adsorbate surface coverage on nanotubes dispersed in aqueous solution decreases, the emission energy decreases (due to an increase in the dielectric constant from water exposure). Upon dilution of a solution of sodium dodecyl sulfate (SDS) suspended SWNT below the critical micelle concentration (cmc), the fluorescence energy systematically decreases; emission exhibits a surfactant concentration-dependent red-shift.[11]

DNA is highly polymorphic and several types of single[3] and double stranded oligonueclotides adsorb to the surface of SWNT. In a previous study,[9] we found that divalent ions optically modulate SWNT PL when the nanotube is wrapped using a GT repeating 30-nucleotide. The modulation has an ion selectivity that is identical to the B to Z form transition for the corresponding free DNA. With increasing concentration, the PL emission wavelength of the SWNT traces a two state equilibrium curve that coincides closely with this B−Z form transition for the corresponding free DNA strand as monitored by circular dichroism. The transition on the SWNT is also thermodynamically reversible: selective removal of the ions via a 12−14 kDa membrane restores the initial optical state. A mathematical and conceptual model that assumes identical DNA transitions on and off the SWNT describes several key features of these data. However, the exact molecular mechanism that proceeds on the nanotube surface is unknown at this time and is the focus of the current work.

DNA is known to adopt various conformations, including the right-handed A, B, C, D form and left-handed Z form.[12] In contrast to B-DNA, the Z-DNA form lacks a major groove. The purine 6, 7, and 8 positions and the pyrimidine 4 and 5 positions are exposed to the external solvent in Z-DNA. Both natural DNA and a variety of synthetic DNA of simple repetitive sequences are capable of adopting more than one conformation. Base sequence rather than overall base composition often clearly influences the preferred conformation under a given set of conditions. Moreover, Pohl and Jovin observed that the circular dichroism (CD) spectra of (poly(dG-dC)·poly(dG-dC)) indicate a B to Z transition when the polymer was exposed to high salt concentrations.[13] Generally speaking, oligomers tend to be in the left-handed conformation in the presence of multivalent cations[14] such as Mg^{2+}, $Co(NH_3)_6^{3+}$, and spermidine^{3+}. It is reported that Mg^{2+} can coordinate directly to N7 of guanine and can hydrogen bond through its hydration sphere to a phosphate oxygen, stabilizing the Z conformation.[15,16] The stability of one DNA conformation is influenced by both the anions and cations.[14]

* E-mail: strano@mit.edu.
[†] Department of Chemical Engineering, Massachusetts Institute of Technology.
[‡] Department of Chemical Engineering, Massachusetts Institute of Technology.
[§] Department of Physics, University of Illinois-Urbana/Champaign.
[||] Division of Biophysics of Macromolecules, German Cancer Research Center.

10.1021/ma070608t CCC: $37.00
Published on Web 08/08/2007

Understanding how the diverse mechanisms of DNA conformational polymorphism are influenced upon adsorption to the nanotube surface is important for several reasons: DNA oligonucleotides have been effective handles to manipulate SWNT.[17,18] They also provide a unique scaffold for sensors and electronic applications.[19] In this work, we investigate the precise molecular mechanism for the optical transduction of DNA conformational polymorphism on carbon nanotubes. We first identify and image the helical or corrugated structure of the DNA-nanotube complex for several sequences via atomic force microscopy in both dry and aqueous environments. The photoluminescence wavelength shift upon cation binding is measured on complexes composed of various oligonucleotide sequences, a 30-base $d(GT)_{15}$, a 30-base $d(GC)_{15}$ and a random sequence of 5′-TAG CTA TGG AAT TCC TCG TAG GCA-3′ (henceforth called DNA1), and exhibits sequence-dependent differences in response. We observe that the transition can be induced thermally as well as ionically and dynamic light scattering (DLS) indicates no aggregation or inter-particle complex formation upon ion addition. Interestingly, the PL red shift induced by ions is not reversible for some sequences if dialysis membranes with large molecular weight cutoff are utilized (100 kDa) to remove the ions. If smaller pore membranes (12−14 kDa) are utilized, as in earlier work,[9] the transition remains reversible with ion removal. We hypothesized that the mechanism involved a dissociation of a DNA that could then permeate the larger but not the smaller dialysis membrane, creating the observed irreversibility. A 20% PAGE gel electrophoresis method confirms this mechanism. We conclude that the conformational change involves a stepwise partial desorption of DNA from the SWNT surface.

Materials and Methods

DNA Encapsulation of Single-Walled Carbon Nanotubes. Single-walled HiPco carbon nanotubes (Rice University) were suspended with three different kinds of DNA (Integrated DNA Technologies, Inc.) sequences, a 30-base $d(GT)_{15}$, a 30-base $d(GC)_{15}$ and 5′-TAG CTA TGG AAT TCC TCG TAG GCA-3′ (henceforth called DNA1), in a 1:1 mass ratio in 0.1 M NaCl in distilled water and bath sonicated for 1 h. The mixture was centrifuged for 90 min at 16 300 g and the pellet discarded. The supernatant was then dialyzed against 1× Tris Buffer at pH 7.4, using 100 kDa molecular weight cutoff dialysis tubing (Spectrum Laboratories Inc., Rancho Dominguez, CA) for 3−5 days, to remove the free DNA, producing the DNA-SWNT samples used in the experiments.

DNA-SWNT Structural Study by Atomic Force Microscopy. Atomic Force microscope (AFM) samples were prepared by depositing $d(GT)_{15}$-SWNT and DNA1-SWNT on freshly cleaved mica. Dry AFM measurements were made by first exposing the mica surface to 1 M $MgCl_2$ and drying with ultrapure nitrogen before depositing $d(GT)_{15}$-SWNT solution at a concentration of 5−10 mg/L. Samples imaged in fluid were prepared by depositing the $d(GT)_{15}$-SWNT solution onto the mica and adding 1 M $MgCl_2$ into a Veeco Fluid Cell. A Digital Instruments Mutimode AFM in tapping mode was used for all measurements. The 3D images were generated using SPIP from Image Metrology.

Aggregation Test by Dynamic Light Scattering. DLS measurements were taken using a Brookhaven Instruments BI-200 SM goniometer, with a Lexel argon ion (model 95) 514 nm laser at a detector angle of 90°. Correlation curves of $d(GT)_{15}$-SWNT and $d(GC)_{15}$-SWNT, with and without $HgCl_2$ (1 mM), were compared using first and second delay times of 0.8 μs and 1s respectively. The diffusion coefficients were determined from a semilogarithmic plot of the autocorrelation function against time: $\ln(G(\tau) - A) = \ln(B) - 2\Gamma\tau$, using the initial linear region where $G(\tau)$ is the correlation function, τ is the time, Γ is the decay rate of the correlation function, A is the baseline intensity, and B is an instrument parameter. The relaxation rate $\Gamma = q^2D$ is related to the diffusion coefficient D[20], and q is

$$q = \frac{4\pi n}{\lambda} \sin\left(\frac{\theta}{2}\right)$$

where $n = 1.33$ is the index of refraction for water, $\lambda = 514$ nm is the wavelength of the laser, and $\theta = 90°$ is the angle between the laser path and the detector.

Alternatively, the correlation curves were analyzed by the maximum entropy method,[21,22] which computes the most probable distribution of relaxation times fitting the autocorrelation function. The analysis was done using the Maxent program developed in the Langowski group.[23] The relaxation times τ given by that program are the inverse of the relaxation rates Γ and proportional to the diffusion coefficient D.

Ion Binding Response of DNA-SWNT by Photoluminescence Method. DNA-encapsulated SWNT were diluted to concentrations of 5 mg/L buffered with 1× Tris adjusted to a pH of 7.4. Solutions of mercury(II) chloride (Aldrich), cobalt(II) chloride hexahydrate (Acros Organics), calcium chloride (Fisher), copper(II) chloride (Aldrich), and magnesium chloride hexahydrate (EMD Chemicals Inc., Gibbstown, NJ) were introduced to the buffered DNA-SWNT and left to equilibrate at 22 °C for at least 24 h for steady-state experiments. Spectrofluorometry measurements were conducted using a Kaiser Optical Holospec f/1.8 imaging spectrograph (Kaiser Optical, Ann Arbor, MI). A recirculating water bath (Fisher Scientific Inc., Isotemp 1016S) was used to control the temperature.

Temperature-Dependent Thermochromism. A constant temperature cell (63-Q-10, Rectangular, Horizontal Flow Tubes, Starna Cells, Inc.) was used with a water bath (Fisher Scientific Inc., Isotemp 1016S) to cycle the temperature of the purified DNA-SWNT solutions, spectrofluorometry measurements were conducted at 0, 20, and 50 °C. All data were taken when the system reached steady state.

Dissociation of DNA from SWNT. *Dialysis.* Samples were prepared the same way as in the ion binding response for all three kinds of DNA-SWNT. The concentrations of SWNT were kept at 5 mg/L. The transition was induced using Ca^{2+} and Hg^{2+}. The $d(GT)_{15}$-SWNT solution was added with 2.5 mM Ca^{2+} to induce the transition and a further dialysis step against nanopure water was carried out using 100 kDa MW cutoff tubing for 24 h. Furthermore, 0.5 mM Hg^{2+} was used to induce the transitions of $d(GT)_{15}$-SWNT, $d(GC)_{15}$-SWNT and DNA1-SWNT. After an incubation of 24 h, the samples were dialyzed against nanopure water using both 12−14 kDa MW and 100 kDa MW cutoff tubing for 24 h. An extra step of 24 h dialysis using 12−14 kDa MW cutoff tubing was performed after the dialysis using 100 kDa MW cutoff tubing in the case of $d(GT)_{15}$-SWNT incubated with Hg^{2+}.

Gel Electrophoresis. Samples of $d(GC)_{15}$-SWNT and DNA1-SWNT, incubated with 0, 0.2, and 1 mM $HgCl_2$ for 24 h were prepared. The final volume of each sample was 3 μL and the concentration of SWNT was kept the same. A 3 μL of 50 bp DNA ladder (Invitrogen) was used for comparison. A volume of 3 μL of blue/orange 6× loading dye (Promega) was added to each sample. Electrophoresis was performed in a Mini-PROTEAN 3 cell (Bio-Rad Laboratories) at 250 V for 30 min, using a freshly made 20% PAGE gel buffered by 1× TBE at pH 8.5, after a pre-run under 250 V for 15 min. GelStar nucleic acid gel stain (Cambrex) was used to stain the gel for 30 min afterward. Control experiments were done using $d(GC)_{15}$ and DNA1-SWNT, incubated with and without 1 mM $HgCl_2$ for 24 h.

Hybridization Experiment Using FRET. Modified oligonucleotide sequences labeled with the Cy3 fluorophore, biotin, and NH_2 were purchased (HPCL purified) from Integrated DNA Technologies Inc (Coralville, IA). The sequences were 5′-Cy5$(GT)_{15}$Biotin-3′, 5′-$(GT)_{15}$Cy3−3′ and 5′−Cy3-$(GT)_4$G(X)$(GT)_{10}$-3′ where X is an amine bound to C6 on thymine. Oligonucleotide pairs were chosen to allow the formation of either a parallel strand duplex or an antiparallel strand duplex.

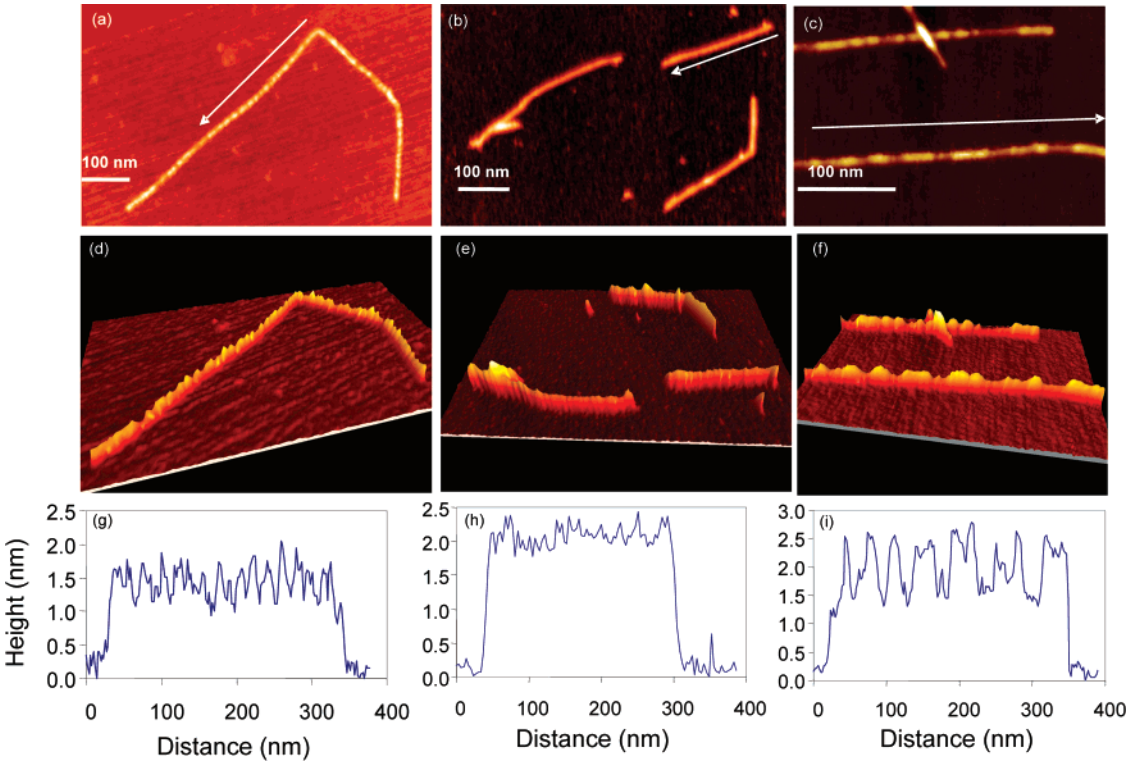

Figure 1. AFM images of DNA-SWNT complexes. (a) AFM height image of $d(GT)_{15}$-SWNT on freshly cleaved mica conducted in air showing regular banding pattern of the $d(GT)_{15}$ oligonucleotide extending up to 0.8 nm above the surface of the nanotube. (b) Wet AFM of $d(GT)_{15}$-SWNT in water shows diminished bands. (c) AFM of DNA1-SWNT in air shows pronounced bands reaching 1 nm above the nanotube surface on average. (d−f) 3D renderings of the micrographs. (g−i) Height profiles of the nanotubes denoted by the white arrows in the original height images.

Sequences were annealed in a 1:1 ratio of 2−4 μM concentrations in 1× Tris pH 8 with 100 mM Na or 1 M Na. They were heated to 85 °C in a PX2 Thermal Cycler (Thermo Electron Corporation, Milford MA) for 10 min, then gradually cooled down to 4 °C over a period of 6 h. The annealed solution at 4 °C was diluted in the 1× Tris pH 8.0 buffer and kept at 4 °C in a chilled quartz cuvette. Fluorescence measurements were performed on the diluted sample by exciting at 535 nm and measuring the emission with a Varian Cary Eclipse Fluorescence spectrophotometer. The temperature was controlled by a Varian Cary Single Cell Peltier accessory (Palo Alto, CA).

Circular Dichroism of DNA on SWNT. Circular dichroism (CD) measurements were taken with a JASCO J-715 spectrometer with temperature control (JASCO International Co. Ltd., Tokyo, Japan) at room temperature unless otherwise specified. Samples were freshly prepared. DI water was used in the dialysis step instead of buffer. Two kinds of experiments were done using CD. Ion-binding response experiment with $d(GT)_{15}$-SWNT and temperature dependence experiment with $d(GT)_{15}$-SWNT and $d(GC)_{15}$-SWNT. For the ion-binding response experiment, CD spectra of $d(GT)_{15}$-SWNT with various concentrations of mercury (II) chloride and calcium chloride were taken. For the temperature dependence experiment, CD spectra of $d(GT)_{15}$-SWNT and $d(GC)_{15}$-SWNT at 20 and 50 °C were taken.

Results and Discussion

Structural Studies of DNA—Nanotube Complexes. AFM measurements of the $d(GT)_{15}$-SWNT complex, conducted in air, show a regular banding pattern along the nanotube (Figure 1, parts a and d). The band heights reach up to 1.2 nm above the surface of the nanotube, with typical heights of 0.7−0.8 nm, and exhibit a regular spacing of 14−20 nm (Figure 1g). Measurements conducted in fluid show greatly diminished banding attributed to the effective increase of DNA's hydrated radius compared to the dehydrated strand (Figure 1, parts b, e, and h). However, DNA1 adsorbs in a globular manner on SWNT, which is apparent in its AFM images in air (Figure 1, parts c and f). The average diameter of DNA1-SWNT complex is estimated as its radius of gyration and calculated to be 1.66 nm ($d = l\sqrt{N}$, where l is the length between adjacent bases and N is the number of bases), assuming the single-stranded DNA chains are behaving as free nonentangled Gaussian chains. This is consistent with the average height that is observed by AFM where the nanotube height is ∼1 nm. The smaller extension of $d(GT)_{15}$ from the nanotube also implies a tighter binding to its surface, and the regular banding pattern suggests a more uniform conformation of the oligonucleotide. These conclusions concur with the observed relative stability of the $d(GT)_x$ oligonucleotide binding to the nanotube.[18]

Ion Induced DNA Conformational Polymorphism. Divalent ions are known to bind to the negatively charged backbone of DNA and induce conformational changes, as in the case of the first-order cooperative transition.[13] The DNA-SWNT complexes demonstrate reversible red shifting of the emission energies of their near-infrared photoluminescence in response to increasing divalent ion concentration.

The response is observed to trace a two state, equilibrium curve, as depicted in Figure 2 for various ions and three different sequences on the SWNT. While all SWNT in the sample demonstrate the PL red shift, the diameter dependence of the trend reported earlier[9] is such that the (6,5) SWNT has the largest shift. We focus on this species for the remainder of the study, while acknowledging similar trends for other SWNT. The maximum photoluminescence red-shift for all sequences is approximately 15 meV upon introduction of Hg^{2+} cations, with smaller shifts seen in response to other ions. Under some conditions, the ion concentration results in weakly attractive inter-particle potentials between DNA-SWNT, and quiescent

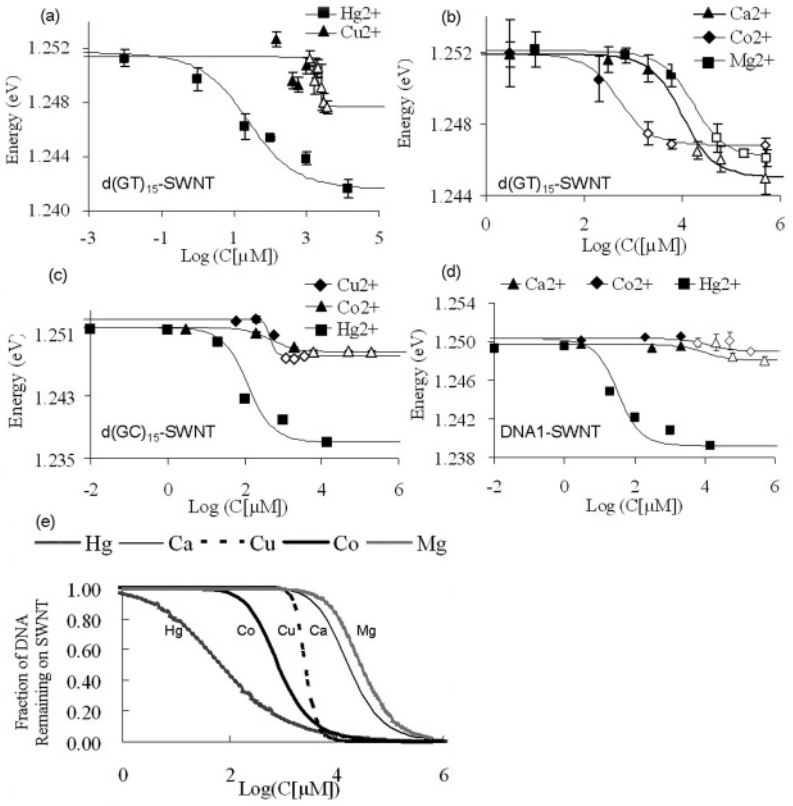

Figure 2. (a−d) Photoluminescence energy of (6,5) nanotube decreases due to the addition of various ions to $d(GT)_{15}$-SWNT (a, b), $d(GC)_{15}$-SWNT (c), and DNA1-SWNT (d). The response is observed to trace a two state, equilibrium curve. Points here indicate data; hollow points indicate loosely held aggregates. Curves show the two-state model developed in the text. (e) The fraction of $d(GT)_{15}$ remains on SWNT on adding the five kinds of ions in this work, predicted by the model.

solutions show loosely assembled aggregates (Open symbols, Figure 2). These aggregates remain photoluminescent and are easily redispersed by simple stirring (no ultrasonic processing). This process does *not* affect the PL wavelength, and is not responsible for the optical modulation. During measurements of divalent ion induced optical modulation, DLS measurements confirmed that no detectable aggregation of the DNA-SWNT occurred after the addition of 1 mM $HgCl_2$ to either $d(GT)_{15}$-SWNT or $d(GC)_{15}$-SWNT (Figure 3b). A maximum entropy evaluation of the autocorrelation functions resulted in the Maxent plots given in Figure 3b with a bimodal distribution in relaxation times $\tau_R = 1/\Gamma$. The analysis found two dominant components. The major component's diffusion coefficient (from $\Gamma = q^2D$) is 4.2×10^{-12} m^2 s^{-1} and a minor fast component is apparent at 2.1×10^{-11} m^2 s^{-1}. Assuming an average nanotube diameter of 1 nm, these correspond to lengths of 600 and 40 nm respectively. In the presence of $HgCl_2$, the plots show no significant change in diffusion coefficient and therefore, no aggregation.

Temperature-Dependent Thermochromism. A red shift of the SWNT PL is observed with an increase in temperature to 50 °C for all three DNA-SWNT (Figure 3a). Cooling below this temperature to 0 °C causes a blue shift. No divalent ions were added in this experiment, proving that the transition can be induced thermally. We anticipate that temperature changes over this range generally induce secondary structural changes in DNA.[14] The observation makes the possibility unlikely that the ion adsorbs and interacts with the SWNT directly. Both temperature and divalent ions alter DNA secondary structure, thus we conclude that the SWNT is modulated by changes in the adsorbed DNA structure.

Dissociation of DNA from SWNT. The red shift observed is not due to aggregation according to DLS, and it is not an ion/SWNT interaction according to the temperature dependent thermochromism results, leaving the secondary structure of DNA as the only possible explanation. To test whether a dissociative mechanism is involved (i.e., desorption of the DNA from the SWNT surface), the following dialysis experiment was performed. The (6,5) nanotube energy of $d(GT)_{15}$-SWNT, $d(GC)_{15}$-SWNT and DNA1-SWNT before and after the introduction of Ca^{2+} or Hg^{2+} was plotted in Figure 4. A further dialysis step using 100 kDa MW cutoff tubing was performed after the transition reached steady state, and it was compared to the result by using 12−14 kDa MW cutoff tubing. Parts b−d of Figure 4 show that for all three sequences the use of 100 kDa MW cutoff tubing to remove the Hg^{2+} results in no return of the blue shift to the starting point. Because the pore size of the membrane determines whether the shift is reversible or irreversible upon ion dialysis, we hypothesize that a dissociative mechanism is involved. Upon ion addition, DNA in single or complex form desorbs from the SWNT. If it is prevented from escaping through the dialysis tubing, the transition remains reversible. Otherwise it is irreversible. The extent or reversibility via the small pore (12−14 kDa) membrane is $d(GT)_{15}$-SWNT > $d(GC)_{15}$-SWNT > DNA1-SWNT. We note that the molecular weight for $d(GT)_{15}$, $d(GC)_{15}$ and DNA1 is 9439.1,, 9213.9, and 7367.8 g/mol, respectively (Supporting Information), meaning that DNA1 has the highest possibility to transport through the 12−14 kDa MW cutoff tubing pore. Moreover, a 24 h dialysis using 12−14 kDa MW cutoff tubing after a 24 h dialysis using 100 kDa MW cutoff tubing did not cause the blue shift back (Figure 4b). Hence, the energy shift is irreversible when the

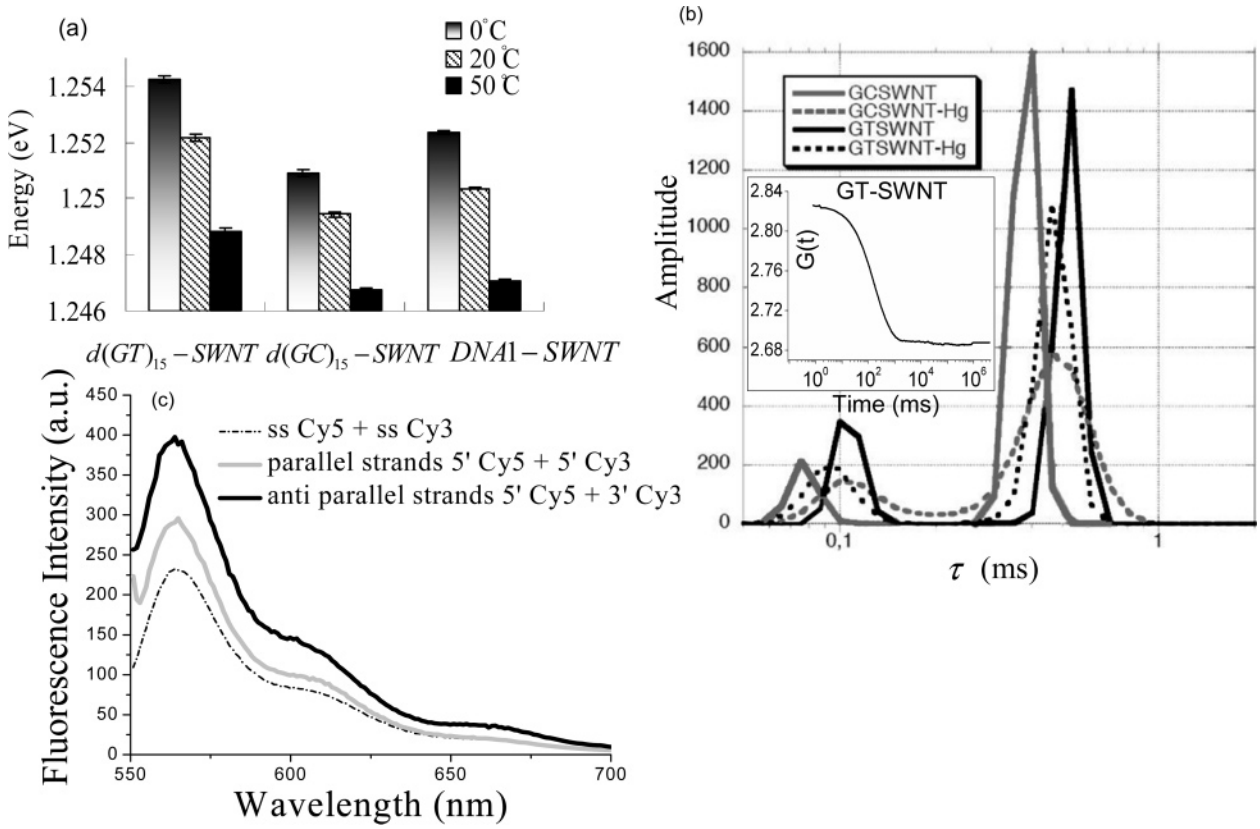

Figure 3. (a) Energy decrease of (6,5) nanotube due to the temperature increase with three different kinds of DNA-SWNT. (b) Dynamic light scattering Maxent plots compiled from correlation curves of DNA-SWNT complexes show no significant change in τ upon addition $HgCl_2$. Inset shows a correlation curve of the GT-SWNT complex. (c) Fluorescence emission of the annealed DNA samples and the control of separate Cy3-ssDNA and Cy5-ssDNA on 535 nm excitation. The lack of Cy5 emission implies that no parallel or antiparallel duplex was formed, and hence no FRET between Cy3 and Cy5 occurred.

system is dialyzed using 100 kDa MW cutoff tubing at any stage. Herein, the transition is proposed as a competitive, partial peeling off of the DNA with increasing divalent ion concentration. DNA removal proceeds in a stepwise manner along the length. The process must complete before total desorption occurs. Compared to other ions, Hg^{2+} binds effectively, and at nanomolar concentrations should facilitate this process. However, for the other ions, complete desorption is not certain for moderate concentration ranges (Figure 2e, see derivation in the two-state model). For example, in the case of $CaCl_2$, the transition remains fully reversible when dialyzing using a 100 kDa MW cutoff tubing for 24 h (Figure 4a).

To validate this dissociative hypothesis, we sought to detect an increase in free solution DNA upon divalent ion addition. A 20% PAGE gel that only allows free DNA to permeate into the gel was utilized. GelStar nucleic acid gel stain was used to detect either double-stranded or single-stranded DNA in gels. GelStar stain is highly fluorescent only when bound to nucleic acids thus giving superior signal-to-noise ratios and obviating the need to destain the gel. The detection limits of GelStar strain are 20 pg for dsDNA and 25 pg for ssDNA.[24] Further, we observed that its fluorescence is not quenched by $HgCl_2$ in the case of $d(GC)_{15}$ (Figure 5b). There are two bands for $d(GC)_{15}$ because this oligonucleotide can self-associate (Figure 5a). The fast band is the single strand band and the slow band is the double strand band. The intensity of the fast band is increased by 23% with 0.2 mM $HgCl_2$ and 55% with 1 mM Hg. Moreover, the length of the slow band is increasing with the concentration of $HgCl_2$ (Figure 5c). On the other hand, the result from DNA1-SWNT is inconclusive in Figure 5a because the dye fluorescence is quenched by $HgCl_2$ (Figure 5b). The sample of $d(GT)_{15}$ is not included here because no fluorescence was observed in this assay.

While $d(GT)_{15}$ does not form the traditional Watson−Crick base pairs, it can form T−T and G−G base pairs by hydrogen bonds.[25] It was discovered by optical techniques that the telomeric $dG(GT)_4G$ sequence can form a parallel-stranded double helical conformation via this nontraditional purine−purine and pyrimidine−pyrimidine base paring.[26] G quadruplexes are formed in this case to stabilize the structure. We have found, however, that the $d(GT)_{15}$ oligonucleotide does not form a duplex based on experimental results using FRET. A $d(GT)_{15}$ oligonucleotide labeled with Cy5 at the 5′ end and a similar strand with 3′ bound Cy3 were annealed in the presence of two different NaCl concentrations. On exciting the annealed sample at the Cy3 absorption maximum of 535 nm, we expect to see a strong Cy5 emission at 664 nm due to FRET between the dye pair if double stranded DNA is formed. The GT annealed product did not produce an emission peak at 664 nm for either parallel or antiparallel duplex formation at 100 mM Na and at 1 M Na (Figure 3c). The small peak visible at ∼660 nm is understood to be Cy5 emission on indirect absorption of the 535 nm incident light. This can be seen in the dotted curve which is the sum of the emission obtained on separately excited Cy3-ssDNA and Cy5-ssDNA. Hence, we conclude GT does not form a parallel or antiparallel duplex in free solution, also confirmed by an experiment involving the intercalating dye PicoGreen (Figure S1). However, we note that on the SWNT surface, it behaves functionally similar to $d(GC)_{15}$ which is a dimer both in free solution and on the SWNT. It is likely that $d(GT)_{15}$ does not have a simple single-stranded structure on the SWNT, despite the evidence that it is dissociated in free

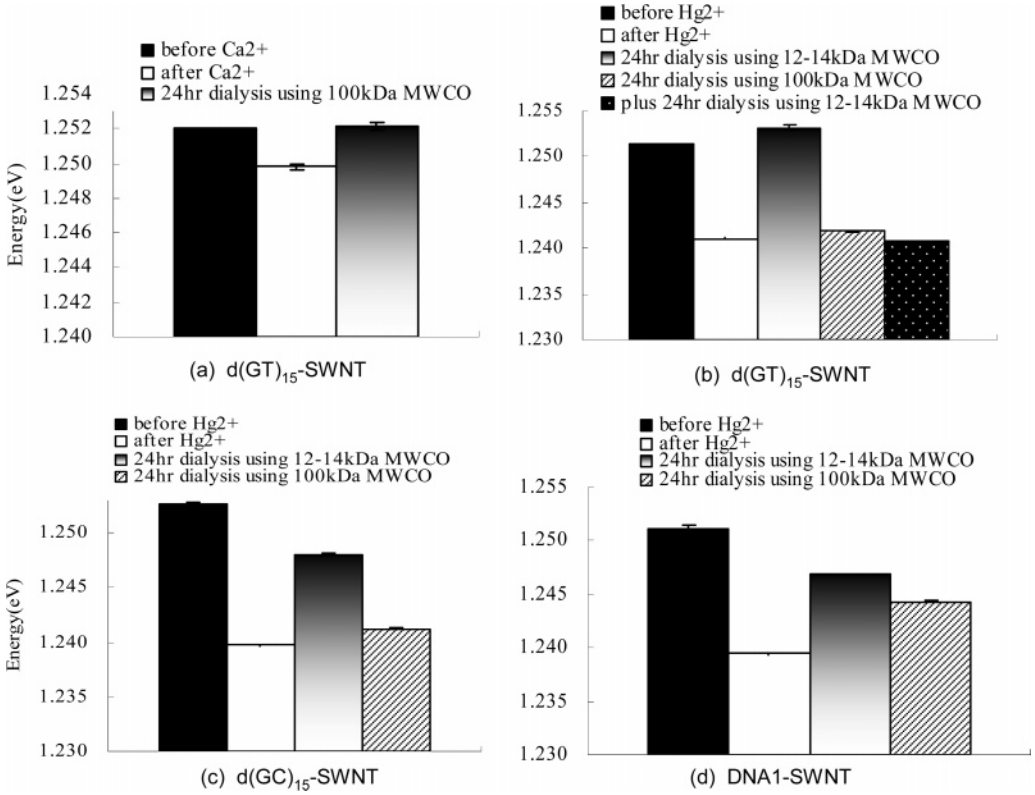

Figure 4. Photoluminescence energy of (6,5) nanotube before and after the introduction of ions to $d(GT)_{15}$-SWNT (a, b), $d(GC)_{15}$-SWNT (c), and DNA1-SWNT (d). A 24 h dialysis was done for experiments with $HgCl_2$ using both 12-14 kDa MWCO and 100 kDa MWCO tubings, (b−d). An extra step of 24 h dialysis using 12-14dDa MWCO tubing is performed after the 24 h dialysis using 100 kDa MWCO tubing for $d(GT)_{15}$-SWNT in part b. A 24 h dialysis was done for experiment with $CaCl_2$ (a), using 100 kDa MWCO tubing. The concentrations for $CaCl_2$ and $HgCl_2$ are 2.5 mM and 0.5 mM respectively.

solution. The sequence we refer to as DNA1 is obviously single-stranded and a duplex is formed only in the presence of its complement sequence.

Herein, we attribute the red shift to the conformational change of DNA on SWNT, which involves a competitive, stepwise partial peeling off of the DNA along the length. However, circular dichroism spectra of DNA while adsorbed to the SWNT surface,[27] show no change either on adding ions (Figure 6, parts a and b, the decreasing intensity is due to the dilution) or changing temperature (Figure 6, parts c and d). We note here that the peak around 260 nm is characteristic for DNA, depending on the specific DNA sequence, it may shift up to 280 nm.[9,28] Therefore, we focus on the peak from 260 to 280 nm for the structure study with DNA-SWNT. Further, we note that the system remains stable during the transition, which would be unlikely for the case of DNA desorbing significantly. For $d(GC)_{15}$ the emerging picture is one of a duplex DNA dissociating and leaving single-strand DNA on the SWNT (Figure 6e). A similar mechanism is proposed for $d(GT)_{15}$ and DNA1 on SWNT, but instead of involving duplex dissociation, may involve part of DNA desorbing and leaving. All cases can be described by the following two-state model.

DNA Conformational Polymorphism Model. In summary, the photoluminescence wavelength shift upon cation binding is measured on SWNT complexes wrapped using three types of oligonucleotide sequences. We verify that the PL shift reflects a conformational change of DNA on SWNT by confirming that transitions can be induced thermally as well as ionically, and by ruling out aggregation as a cause. We further performed dialysis experiments, which show that the PL red shift induced by ions is not fully reversible after dialyzing for 24 h using a 100 kDa MW cutoff tubing. However, a 12−14 kDa molecular weight cutoff tubing yields a molecular weight dependent blue shift. With further proof that free DNA desorbs and leaves by gel electrophoresis, the transition is attributed to a conformational change of DNA on SWNT which involves a competitive, stepwise partially peeling off of the DNA along the length. We propose the following two-state quantitative model, without any structural assumptions of DNA on SWNT.

We assume that it takes β steps for the complete peeling of DNA from SWNT. In the stepwise peeling process, there exist β states of DNA on SWNT described as $DNA_i - \theta_{\beta-i} (i = 0, 1, ..., \beta - 1)$, where DNA_i represents the part of DNA that is released from its binding sites on SWNT (vacuuming i binding sites), $\theta_{\beta-i}$ represents the binding sites on SWNT occupied by the other part of DNA (Given a total number of β binding sites per SWNT, if i of them are empty, $\beta - i$ of them are still occupied). We note here that the physical meaning of β can be considered as the number of binding sites per SWNT, based on Langmuir isotherm theory. However, this "binding site" is theoretical and is different from the actual physical binding site, which depends on the length and sequence of DNA and its chemical bonding with SWNT. No assumption of exact structure of DNA (like double or single strand) is made here so this model can be applied to all three samples of DNA-SWNT in this study (one possibility that DNA is double-stranded on SWNT is shown as an example in Figure 6e).

The β steps of this peeling process can be described in the following reactions.

$$\mathrm{DNA}_i - \theta_{\beta-i} + nI \rightleftarrows \mathrm{DNA}_{i+1} - \theta_{\beta-i-1} \quad 0 \le i \le \beta - 1$$

where n is the number of ions involved in each step.

The overall reaction is obtained by summing the above β reactions together

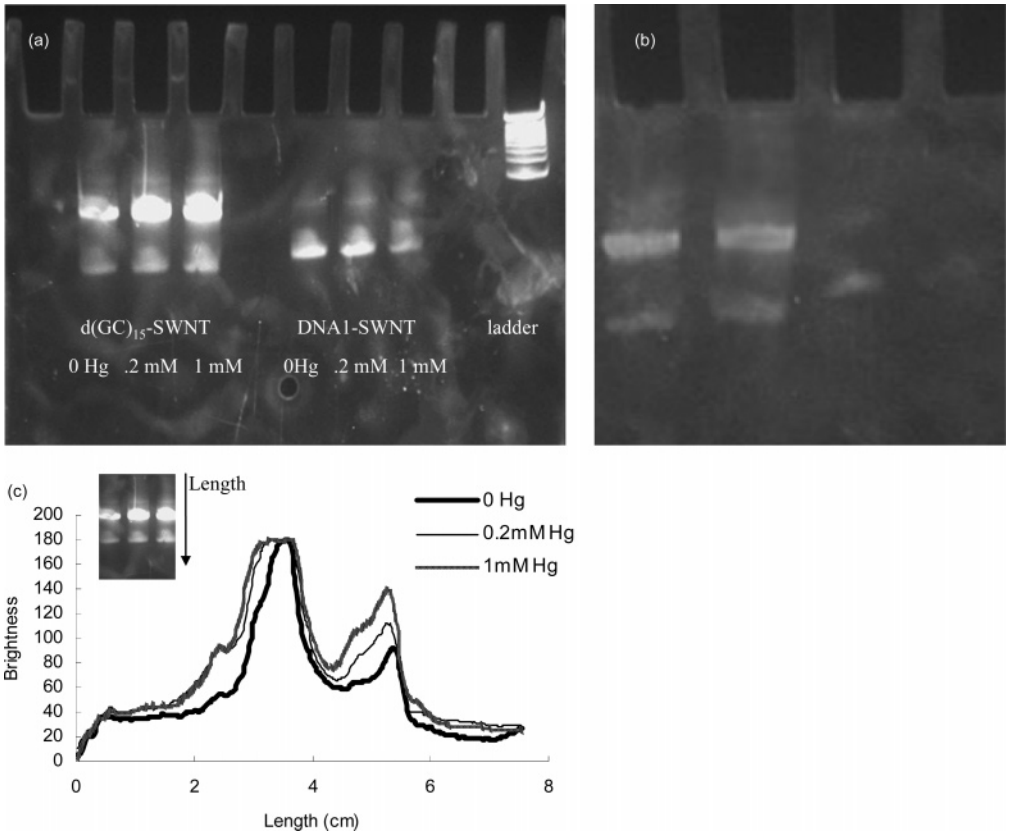

Figure 5. (a) Gel electrophoresis result for d(GC)$_{15}$-SWNT and DNA1-SWNT, incubated with 0, 0.2, and 1 mM $HgCl_2$ for 24 h, compared with a 50 bp ladder. (b) Control experiment where d(GC)$_{15}$ and DNA1, with and without 1 mM $HgCl_2$, shows that $HgCl_2$ quenches DNA1 but not d(GC)$_{15}$. (c) Intensity of brightness of d(GC)$_{15}$-SWNT along the length.

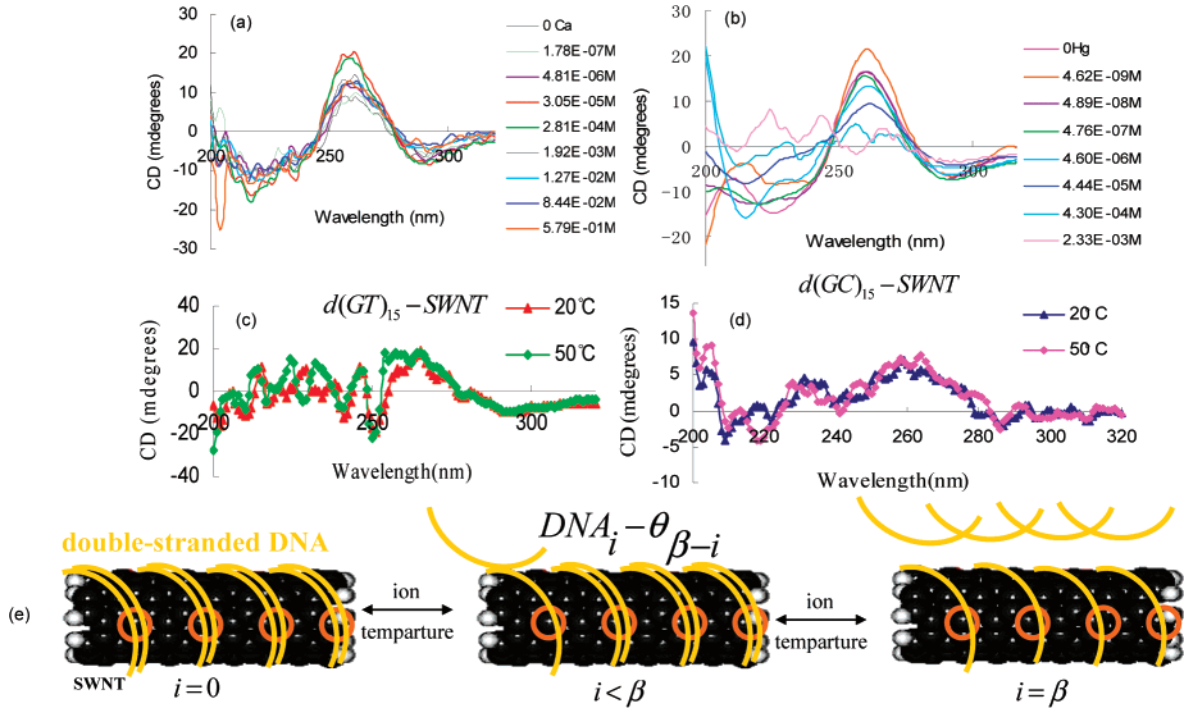

Figure 6. Circular dichroism spectra of d(GT)$_{15}$-SWNT on adding $HgCl_2$ (a) and $CaCl_2$ (b). The spectra show no change. Circular dichroism of d(GT)$_{15}$-SWNT(c) and d(GC)$_{15}$-SWNT(d) at 20 and 50 °C, respectively. They also show no change. Data are smoothed. (e) One sample dissociation mechanism of DNA conformational change on SWNT, which shows single-stranded DNA leaving double-stranded DNA on SWNT. Yellow curves indicate DNA. Black cylinder indicates SWNT. Orange circle indicates the binding site. The number of binding sites released per SWNT is expressed by *i*. The total number of binding sites per SWNT is β.

$$\mathrm{DNA}_0 - \theta_\beta + \beta nI \rightleftarrows \mathrm{DNA}_\beta - \theta_0$$

For convenience, $[\mathrm{DNA}_i - \theta_{\beta-i}]$ is written as *Ai*, which means there are i binding sites released per SWNT. The concentration of ions is written as *I*. We make the assumption here that the forward reaction rate constants (k_1) are identical for the β reaction steps and the backward reaction rate constants (k_{-1})

Table 1. Equilibrium Constants of the Two-State Model for the Three Kinds of DNA-SWNT with Different Ions[a]

	Ca^{2+} M^{-1}	Co^{2+} M^{-1}	Mg^{2+} M^{-1}	Hg^{2+} $M^{-1} \times 10^2$	Cu^{2+} $M^{-3} \times 10^8$ [c]
$d(GT)_{15}$-SWNT	100	2000	60	2 $M^{-0.5}$ [b]	1
$d(GC)_{15}$-SWNT		2000		80	100
DNA1-SWNT	100	80		300	

[a] $\beta = 2$, $n = 1$ for most cases except in the following two cases. [b] $n = 0.5$ for $d(GT)_{15}$-SWNT with Hg^{2+} for better fit. [c] $n = 3$ for $d(GT)_{15}$-SWNT and $d(GC)_{15}$-SWNT with Cu^{2+} for better fit.

are also identical for the β reaction steps. The equilibrium constant for the β reactions equals k_1/k_{-1}, and we use K to represent this. We solve the above β algebraic equations and get (see full derivation in the Supporting Information)

$$A_i = (KI^n)^i A_0 = q^i A_0 \tag{1}$$

where i is an integer, $1 \le i \le \beta$

Let

$$B_0 = \sum_{i=0}^{\beta} A_i = A_0 \frac{1 - q^{\beta+1}}{1 - q} \Rightarrow A_0 = \frac{(1 - q)B_0}{1 - q^{\beta+1}} \tag{2}$$

(B_0 is the total number of SWNT).

The number of total binding sites released for all SWNT in solution is

$$\theta = \sum_{i=0}^{\beta} iA_i \tag{3}$$

Solving eq 1−3 (Supporting Information) we get

$$\theta = \frac{q(1 - (\beta + 1)q^{\beta} + \beta q^{\beta+1})}{(1 - q^{\beta+1})(1 - q)} \cdot B_0 \tag{4}$$

where $q = KI^n$

The DNA surface coverage on SWNT and the normalized energy has the following relation

$$\frac{\Delta E}{\Delta E_{max}} = \frac{\theta}{\beta B_0} = \frac{q(1 - (\beta + 1)q^{\beta} + \beta q^{\beta+1})}{\beta(1 - q^{\beta+1})(1 - q)} \tag{5}$$

The curves in Figure 2a−d show the model. $A_\beta = (KI^n)^\beta A_0$ describes the population of complete transition. According to our hypothesis, A_β/A_0 is the fraction of DNA coming off and $1 - A_\beta/A_0$ is the fraction of DNA that remains on the SWNT. Note that a smaller concentration of Hg^{2+} induces the same amount of transition as other ions in agreement with experiment (Figure 2e).

The ion sensitivity of the PL energy shift depends both upon ion type and sequence. Copper was among the metals found to bind to the bases of DNA with an affinity higher than that of any other divalent cation.[29,30] Cations have the ability to react with a variety of electron-donor sites on polynucleotides. The phosphate moieties of the ribose phosphate backbone and the electron-donor groups on the bases are two main sites of interaction.[31] Some metal ions, such as magnesium ions, prefer the phosphate sites and increase the melting temperature by binding phosphate and stabilizing the double helix. Other ions, such as copper and cobalt, prefer base sites and decrease the melting point by binding to the bases and destabilizing the double helix.[31] In our model, the simplest case is a two step ($\beta = 2$) binding site releasing process. In this case, we float n and K to get the best fit (Table 1). While data fitting leads to $n = 1$ for most ions, the number of ions per step n is 3 for copper and 0.5 for mercury. This is consistent with the fact that copper ions can do both base binding[32] and phosphate binding,[33] and they exhibit the greatest affinity for base among the ions studied among Co^{2+}, Ni^{2+}, Mn^{2+}, Zn^{2+}, Cd^{2+}, and Cu^{2+}. It is reported that Hg^{2+} binds very strongly to the bases, resulting in such a structure where metal ions are strongly held between the two helices of DNA.[30] Also, it is reported in the literature that thymine−Hg−thymine are formed in both single strand DNA and DNA duplexes that contain T residues.[34] This finding is consistent with our model result where n equals 0.5 for Hg with $d(GT)_{15}$-SWNT, and it is feasible that two $d(GT)_{15}$-SWNT strands are linked by one Hg ion. Although some of the metal ions have been considered phosphate binders and others base binders, they do not differ much in the nature of their interaction with DNA.[30] Divalent ions have similar effects upon DNA. They can be placed in a sequence that indicates the magnitude of their influence on DNA structure, as follows: $Mg^{2+} < Co^{2+}$, $Ni^{2+} < Mn^{2+} < Zn^{2+} < Cd^{2+} < Cu^{2+} < Hg^{2+}$.[30] From our experiments, we see that $d(GT)_{15}$–SWNT, $d(GC)_{15}$–SWNT and DNA1-SWNT undergo maximum red shifts of 10, 15, and 11 meV upon addition of $HgCl_2$ and 5, 3, and 1 meV upon addition of $CoCl_2$ (Figure 2a−d). All three samples are the most sensitive to Hg^{2+} ions and the transition is sequence dependent. It is clear that ions are interacting with DNA instead of SWNT, and this is consistent with our proposed model. The PL energy shift depends upon the ion type, with the same order of metal-binding affinities as with free DNA alone. Similar analysis leads us to the ion sensitivity for $d(GT)_{15}$-SWNT as $Mg^{2+} < Ca^{2+} < Co^{2+} < Cu^{2+} < Hg^{2+}$, and it is consistent with that of $d(GC)_{15}$-SWNT and DNA1-SWNT.

Conclusions

The mechanism of optical transduction of DNA conformational polymorphism on single-walled carbon nanotubes (SWNT) induced by the adsorption of divalent cations or temperature cycling is attributed to be a competitive, stepwise process of partial desorption of the DNA along the length of SWNT, since the transition can be induced thermally as well as ionically and dynamic light scattering (DLS) shows no aggregation. Further dialysis experimentation suggests a DNA dissociation mechanism. Free dissociated DNA is detected by gel electrophoresis. A two-state model is derived for comparison with different ions and DNA sequences. All three sequences are the most sensitive to $HgCl_2$, with an ion sensitivity in the order $Mg^{2+} < Ca^{2+} < Co^{2+} < Cu^{2+} < Hg^{2+}$.

Acknowledgment. The authors thank N. Mücke, Division of Biophysics of Macromolecules, German Cancer Research Center, Heidelberg, Germany, for help with AFM experiments and N. K Varde, Department of Chemical and Biomolecular Engineering, University of Illinois-Urbana/Champaign, for experimental assistance. This work was funded by the National Science Foundation, a Beckman Young Investigator award, and a 3M Untenured Faculty Award to Michael S. Strano.

Supporting Information Available: Text containing the full mathematical derivation for the model and details on supporting experiments, including a figures showing the PicoGreen fluores-

cence intensity study. This material is available free of charge via the Internet at http://pubs.acs.org.

References and Notes

(1) Heller, D. A.; Baik, S.; Eurell, T. E.; Strano, M. S. *Adv. Mater.* **2005**, *17*, 2793−2799.
(2) Barone, P. W.; Baik, S.; Heller, D. A.; Strano, M. S. *Nat. Mater.* **2005**, *4*, 86−92.
(3) Jeng, E. S.; Moll, A. E.; Roy, A. C.; Gastala, J. B.; Strano, M. S. *Nano. Lett.* **2006**, *6*, 371−375.
(4) O'Connell, M. J.; Bachilo, S. M.; Huffman, C. B.; Moore, V. C.; Strano, M. S.; Haroz, E. H.; Rialon, K. L.; Boul, P. J.; Noon, W. H.; Kittrell, C.; Ma, J. P.; Hauge, R. H.; Weisman, R. B.; Smalley, R. E. *Science* **2002**, *297*, 593−596.
(5) Misewich, J. A.; Martel, R.; Avouris, P.; Tsang, J. C.; Heinze, S.; Tersoff, J. *Science* **2003**, *300*, 783−786.
(6) Barone, P. W.; Baik, S.; Heller, D. A.; Strano, M. S. *Nat. Mater.* **2005**, *4*, 86−96.
(7) Barone, P. W.; Parker, R. S.; Strano, M. S. *Anal. Chem.* **2005**, *77*, 7556−7562.
(8) Barone, P. W.; Strano, M. S. *Angew. Chem., Int. Ed.* **2006**, *45*, 8138−8141.
(9) Heller, D. A.; Jeng, E. S.; Yeung, T. K.; Martinez, B. M.; Moll, A. E.; Gastala, J. B.; Strano, M. S. *Science* **2006**, *311*, 508−511.
(10) Choi, J. H.; Strano, M. S. *Appl. Phys. Lett.* **2007**, *90*, 223114−223113.
(11) Strano, M. S.; Moore, V. C.; Miller, M. K.; Allen, M. J.; Haroz, E. H.; Kittrell, C.; Hauge, R. H.; Smalley, R. E. *J. Nanosci. Nanotechnol.* **2003**, *3*, 81−86.
(12) Zimmerman, S. B. *Annu. Rev. Biochem.* **1982**, *51*, 395−427.
(13) Fritz, M.; Pohl, T. M. J. *J. Mol. Biol.* **1971**, *67*, 375−396.
(14) Jovin, T. M.; Soumpasis, D. M. *Annu. Rev. Biochem.* **1987**, *38*, 521−560.
(15) Wang, A. H.-J.; Quigley, G. J.; Kolpak, F. J.; Marel, G. V. D.; Boom, J. H. V.; Rich, A. *Science* **1981**, *211*, 171−176.
(16) Gessner, R. V.; Quigley, G. J.; Wang, A. H. J.; Van der Marel, G. A.; Van Boom, J. H.; Rich, A. *Biochemistry* **1985**, *24*, 237−240.
(17) Zheng, M.; Jagota, A.; Semke, E. D.; Diner, B. A.; McLean, R. S.; Lustig, S. R.; Richardson, R. E.; Tassi, N. G. *Nat. Mater.* **2003**, *2*, 338−342.
(18) Zheng, M.; Jagota, A.; Strano, M. S.; Santos, A. P.; Barone, P.; Chou, S. G.; Diner, B. A.; Dresselhaus, M. S.; McLean, R. S.; Onoa, G. B.; Samsonidze, G. G.; Semke, E. D.; Usrey, M.; Walls, D. J. *Science* **2003**, *302*, 1545−1548.
(19) Staii, C.; Johnson, A. T. *Nano. Lett.* **2005**, *5*, 1774−1778.
(20) Berne, B. J.; Pecora, R. *Dynamic light scattering: with applications to chemistry, biology, and physics*; Dover Publications: Mineola, NY, 2000.
(21) Bryan, R. K. *Eur. Biophys. J.* **1990**, *18*, 165−174.
(22) Langowski, J.; Bryan, R. *Macromolecules* **1991**, *24*, 6346−6348.
(23) Modos, K.; Galaantai, R.; Baardos-Nagy, I.; Wachsmuth, M.; Toth, K.; Fidy, J.; Langowski, J. *Eur. Biophys. J. Biophys. Lett.* **2004**, *33*, 59−67.
(24) White, H. W.; Vartak, N. B.; Burland, T. G.; Curtis, F. P.; Kusukawa, N. *Biotechniques* **1999**, *26*, 984−988.
(25) Beschetnova, I. A.; Kaluzhny, D. N.; Livshits, M. A.; Shchyolkina, A. K.; Borisova, O. F. *J. Biomol. Struct. Dyn.* **2003**, *20*, 789−799.
(26) Shchyolkina, A. K.; Borisova, O. F.; Livshits, M. A.; Klement, R.; Jovin, T. M. *J. Biomol. Struct. Dyn.* **2001**, *18*, 493−504.
(27) Dukovic, G.; Balaz, M.; Doak, P.; Berova, N. D.; Zheng, M.; McLean, R. S.; Brus, L. E. *J. Am. Chem. Soc.* **2006**, *128*, 9004−9005.
(28) Fasman, G. D. *Circular Dichroism and the Conformational Analysis of biomolecules*, 1st ed.; Plenum Press: New York, 1996.
(29) Geierstanger, B. H.; Kagawa, T. F.; Chen, S. L.; Quigley, G. J.; Ho, P. S. *J. Biol. Chem.* **1991**, *266*, 20185−20191.
(30) Gunther, L.; Eichhorn, Y. A. S. *J. Am. Chem. Soc.* **1968**, *90*, 7323−7328.
(31) Eichhorn, G. L. *Nature* **1962**, *194*, 474−475.
(32) Sara, E.; Bryan, E. F. *Biochemistry* **1967**, *6*, 2728−2734.
(33) James, J. Butzow, G. L. E. *Biopolymers* **1965**, *3*, 95−107.
(34) Miyake, Y.; Ono, A. *Tetrahedron Lett.* **2005**, *46*, 2441−2443.

MA070608T